

# Control of vortex-induced non-resonance vibration using piezo-ceramic actuators embedded in a structure

M M Zhang, L Cheng and Y Zhou

Department of Mechanical Engineering, The Hong Kong Polytechnic University, Hung Hom, Kowloon, Hong Kong

E-mail: [mmlcheng@polyu.edu.hk](mailto:mmlcheng@polyu.edu.hk)

Received 17 December 2004, in final form 9 July 2005

Published 11 October 2005

Online at [stacks.iop.org/SMS/14/1217](http://stacks.iop.org/SMS/14/1217)

## Abstract

Closed-loop control of vortex-induced non-resonant vibration of a flexible square cylinder is experimentally investigated in this paper. Piezo-ceramic actuators were embedded inside the cylinder to cause an oscillation of the cylinder surface, which subsequently altered the fluid–structure interaction. Experiments were conducted in a wind tunnel at Reynolds numbers,  $Re$ , of 2800 and 8000. Two typical control schemes, i.e.  $Y$ -control and  $u + Y$ -control, were deployed using feedback signals from structural vibration  $Y$  and combined  $Y$  and fluctuating flow velocity  $u$ , respectively. The control effects on the structural vibration and flow were assessed using a laser vibrometer, an optical fiber Bragg grating sensor, hot wires and particle image velocimetry. Experimental results show that both vortex shedding from the cylinder and the vortex-induced non-resonant vibration were effectively suppressed. The best control effects were observed with  $u + Y$ -control in use; the root mean square values of  $Y$ , the structural strain rate  $\varepsilon_y$  along the lift direction and  $u$ , i.e.  $Y_{\text{rms}}$ ,  $\varepsilon_{y,\text{rms}}$  and  $u_{\text{rms}}$ , and the circulation  $\Gamma$  dropped at  $Re = 8000$  by 58%, 52%, 53% and 88%, respectively, compared with the unperturbed case. It was found that the control effectively modified the nature of the fluid–structure interaction by changing the in-phase fluid–structure synchronization at all dominant frequencies into anti-phase interaction, accounting for the suppression in both vortex shedding and structural vibration.

## 1. Introduction

Steady cross-flow incident on a bluff body is frequently seen in engineering. When the Reynolds number  $Re$  ( $\equiv U_\infty h/\nu$ , where  $U_\infty$  is the free-stream velocity,  $h$  is the characteristic height of a structure and  $\nu$  is the kinematic viscosity of fluid) exceeds a critical value, the shear layers on both sides of the structure may separate alternately from the structure, forming an unsteady flow pattern, known as the Kármán vortex street. The vortices are quasi-periodic in nature, thus exciting the structure to oscillate. On the other hand, the structural oscillation in turn alters the flow field, resulting in a fluid–structure coupling. This vortex-induced structural vibration problem is commonly seen in many engineering applications, such as in offshore structures, heat exchangers, nuclear power

plants, power transmission cables and bridges; it may cause noise, affect the fatigue life of structures and even result in structural damage. Therefore, understanding and controlling vortex-induced structural vibration has attracted great attention in the past (Bearman 1967, Griffin and Ramberg 1975, Unal and Rockwell 1988a, Williamson and Roshko 1988, Mittal and Kumar 2001, Sarpkaya 2004).

Existing control strategies can be roughly classified as flow control and structural vibration control. The former targets only vortex shedding and subsequently suppresses vortex-induced vibration, while the latter directly controls the structural vibration. For flow control, a considerable amount of work was conducted using passive control, such as changing the structural geometry (Zdravkovich 1981), attaching grooves or riblets on structural surfaces (Owen *et al* 2001) and placing a

splitter plate behind the structure (Unal and Rockwell 1988b). With the advent of fast digital processing and state-of-the-art actuators, active control, involving the input of energies via the actuators to bring about desirable changes to the flow structure system, has recently been given due attention in the literature. Most existing investigations are focused on flow control; various techniques have been deployed, e.g. using acoustic excitation (Blevins 1985, Ffowcs Williams and Zhao 1989, Hsiao and Shyu 1991, Roussopoulos 1993), oscillating or rotating cylinders (Koopman 1967, Tokumaru and Dimotakis 1991, Filler *et al* 1991) and surface bleeding (Williams *et al* 1992, Min and Choi 1999), introducing high frequency spanwise oscillatory cross-flow or oscillatory motion of the channel wall to control a turbulent channel flow (Jung *et al* 1992) and injecting air bubbles to reduce the skin-friction drag in the turbulence boundary layer (Winkel *et al* 2004).

In the past decade, technologies using smart materials have become the enabler that cuts across traditional boundaries between material science and engineering. Smart technology, including sensors, actuators and controllers, has given rise to a broad spectrum of research and applications, and offers new possibilities for flow and structural vibration control. While the smart material technology, especially advanced piezo-ceramic actuators, has made an impact upon structural vibration control (Yang and Chen 1996, Halim and Moheimani 2002, Gao and Cheng 2004), there have been relatively few investigations aimed at integrating sensing and actuating elements into a flow structure system to form an integrated vortex-vibration-free structure. Baz and Kim (1993) and Tani *et al* (1999) made attempts to control the vibration of a cylinder in a cross-flow. In their works, surface-bonded piezo-ceramic patches were activated by a closed-loop control system to exert a force on the cylinder under resonance, that is, the vortex shedding frequency coincided with the natural frequency of the cylinder. The control increased the flow structure system damping and subsequently reduced the vortex-induced vibration. Recently, Cheng *et al* (2003) developed a ‘smart cylinder’ with piezo-ceramic actuators embedded underneath the structural surface of a rigid square cylinder. The excitation of these actuators created a surface perturbation, which drastically altered the fluid–structure interaction given an appropriate excitation signal. The performance of the control system was greatly enhanced with the deployment of a closed-loop control (Zhang *et al* 2004), with the structural vibration and the vortex strength dropping by 82% and 70%, respectively, compared with the case without control.

Apart from Baz and Kim (1993), most previous investigations targeted rigid cylinders on flexible supports and neglected the flexural nature of an engineering structure, which implies multiple degrees of freedom when vibrating. As a result, only the first mode of vibration could be considered. However, the higher modes of structural vibration can be far more violent than the first-mode vibration (Zhou *et al* 2001). Furthermore, previous investigations were mostly focused on the resonance case; there has been a lack of reports on the control of the non-resonance vibration of a structure in a cross-flow. In practice, the occurrence of resonances can be avoided in a reasonable design of engineering structures; for instance, this may be achieved, under a given flow condition, by properly choosing structure parameters relating to its mass and stiffness,

which determine the natural frequencies of the structure. As such, most engineering structures are operated under non-resonant conditions. Nevertheless, this non-resonant vibration is often persistent and can be excessive. As a matter of fact, in the context of flow-induced vibrations, the non-resonance vibration can have an amplitude well exceeding that of the first-mode resonance given a considerably higher reduced velocity (Zhang *et al* 2003). Therefore, the non-resonance vibration can have a significant impact on the fatigue life of engineering structures in the long run. The control of the non-resonant vibration is far more challenging, compared with resonant cases, for both passive and active control. For example, resonant vibrations can be easily reduced by adding damping to the system; however, the non-resonant vibration is insensitive to the damping treatment. In addition, vibrations at resonance are mostly dominated by one mode, but the non-resonant vibrations of engineering structures in general involve responses from various modes, which increases to a great extent the degree of difficulty in control.

This work aims to investigate the effectiveness of the perturbation technique, used by Zhang *et al* (2004), for flexural structures in a cross-flow under non-resonance conditions. The working principle of the perturbation technique and the characteristics of the embedded piezo-ceramic actuators are first described. Two closed-loop control schemes are considered and compared, which use feedback signals from structural vibration ( $Y$ ) and a combination of  $Y$  and the streamwise fluctuating flow velocity ( $u$ ). Control performances are evaluated in terms of suppressing the structural oscillation and vortex shedding, based on the measurements of time histories and power spectral density functions of  $Y$ , dynamic strain  $\varepsilon_y$  and  $u$ , flow visualization and the iso-contours of vorticity. These data were obtained using a hot wire, a laser vibrometer, an optical fiber Bragg grating (FBG) sensor (Zhou *et al* 1999) and a particle image velocimeter (PIV). In order to understand the underlying physics, the effect of the spectral phase between  $u$  and  $Y$  on the control effect is also discussed.

## 2. Perturbation technique and THUNDER actuator

Given a sufficiently large Reynolds number, steady flow incident on a bluff body develops into an unsteady wake and vortex shedding from the bluff body results from the initially linear wake instability, that is, the vortex structure depends on its infant form. Local perturbations to the flow, when small enough to comply with the linear theory (Provansal *et al* 1987), may grow exponentially. Thus, small local perturbations to the flow may exert a significant influence on the unsteady Kármán vortex street. Although the physics involved is not fully understood, there is strong evidence that weak perturbations do influence vortex shedding in the highly non-linear unsteady wake, and this influence can sometimes be dramatic. Typical examples of the impact of small local perturbations upon vortex shedding may be seen in Hsiao and Shyu (1991), Williams *et al* (1992), Huang (1996) and Zhang *et al* (2004). The fact that vortex shedding is sensitive to the local perturbation may naturally influence vortex-induced structural vibrations since vortex shedding is the excitation source of the vibrations. If an appropriate local perturbation on the cylinder surface is created

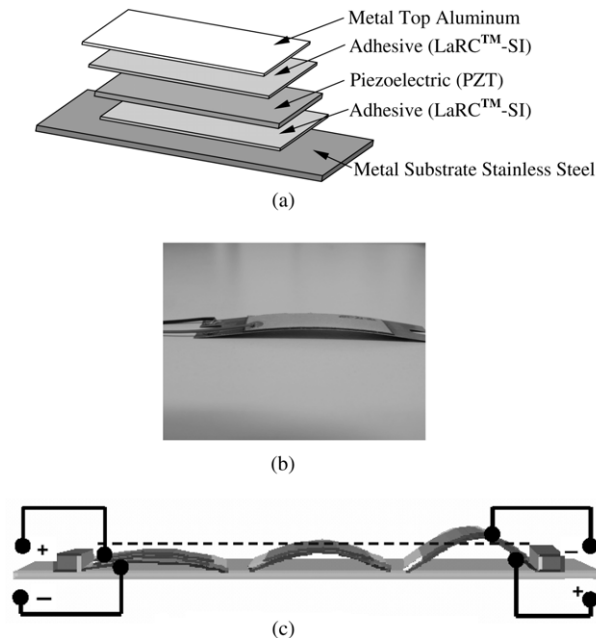


**Figure 1.** Description of THUNDER actuators: (a) THUNDER construction; (b) photo of THUNDER; (c) typical deformation versus applied voltage.

to modify the fluid–structure interaction, both vortex shedding and its induced vibration may be controlled simultaneously. The two-dimensional local perturbation can be introduced to the flow field by the lateral motion of a portion of the cylinder surface with an amplitude much less than that of the structural vibration, which can be excited by an agent embedded in the structure, such as actuators. This moveable cylinder surface can be a plate supported by the actuators and flush with the cylinder surface. Once actuated, the plate can move up and down with the actuators. On the basis of this idea, a novel technique, referred to as the surface perturbation technique, is developed using a new type of advanced piezo-ceramic actuator, called THUNDER (THin layer composite UNimorph piezoelectric Driver and sEnsoR).

THUNDER, developed by NASA Langley research center in 1996, is a composite, consisting of a metal base layer, a piezoelectric layer in the middle and an aluminum foil on the top. LaRC™-SI adhesive is applied between the layers (figure 1(a)). The layers, being specially fabricated (Copeland *et al* 1999), are internally ‘pre-stressed’, resulting in the characteristic bend or curvature of the finished product (figure 1(b)). This gives THUNDER some appealing features such as larger displacement and load capacity than conventional piezoelectric actuators. Under an applied voltage, the actuator deforms out of plane (figure 1(c)). The THUNDER actuator used in the present work was model TH 8-R, which may vibrate at a maximum displacement of about 2 mm within a frequency range up to 2 kHz in the absence of loading and may produce a force up to 67 N.

Figure 2 shows the installation of actuators in a square cylinder, which is used as a test model. Once excited, the actuators may drive one surface of the cylinder to oscillate in a direction normal to the cross-flow. This oscillation may modify

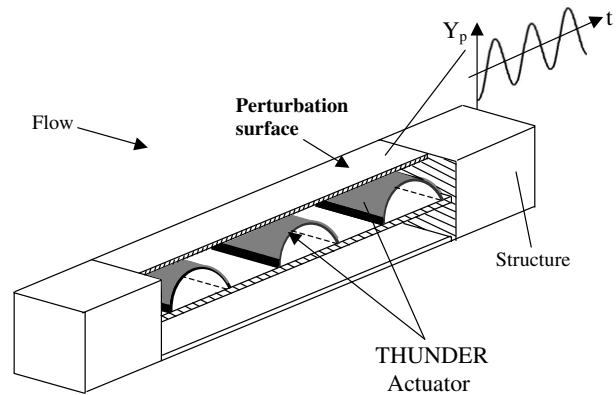


**Figure 2.** Embodiment of the perturbation technique.

interactions between the flow and the cylinder, thus altering the vortex shedding or vortex-induced structural vibration.

### 3. Experimental set-up

Experiments were carried out in a closed-circuit wind tunnel with a 2.4 m long square working section (0.6 m × 0.6 m). A flexible square cylinder, made of nylon, of height  $h = 17.3$  mm was fix-supported at both ends and placed 0.2 m downstream of the exit plane of the tunnel contraction, as shown in figure 3(a). Once excited, the cylinder may vibrate at multiple degrees of freedom. Three THUNDERs were embedded in series in a slot on one side of the cylinder to support a thin plastic plate, which was flush with the cylinder surface (see the cut-away view in figure 3(b)). Driven by the actuators, the plastic plate moved up and down to provide the desired surface perturbation. Detailed information on the installation of the actuators was given in Cheng *et al* (2003). Experiments were done at the free-stream velocities  $U_\infty = 2.5$  and  $7$  m s<sup>-1</sup>, corresponding to  $Re = 2800$  and  $8000$ , respectively. The natural vortex shedding frequency  $f_s$  at  $Re = 2800$  was 21 Hz, lower than the first-mode natural frequency of the cylinder  $f'_n = 47.9$  Hz, and 58 Hz at  $Re = 8000$ , between  $f'_n$  and the third-mode natural frequency of the cylinder  $f'''_n (=174.2$  Hz). Here,  $f'_n$  and  $f'''_n$  were determined from the frequency response of the cylinder vibration when excited with an electromechanical shaker under the no flow condition.

A  $5 \mu\text{m}$  tungsten hot wire (hot wire ⊙) was placed at  $x/h = 0$ ,  $y/h = 1.5$  and  $z/h = 5$  to measure the streamwise fluctuating flow velocity ( $u_1$ ). The coordinates  $x$ ,  $y$  and  $z$  are along the streamwise, transverse and spanwise directions, respectively, with their origin at the center of the mid-span cylinder. The cylinder vibration displacement ( $Y$ ) was measured using a laser vibrometer (Polytec OFV3100). Structural strain,  $\varepsilon_y$ , due to the flexural deformation of the cylinder associated with  $Y$  was monitored by a fiber Bragg grating (FBG) sensor, buried in a groove at mid-span of the cylinder, flush with the surface, using nail polish (figure 3(a)). The FBG sensor was holographically written on an optical silicon fiber with a diameter of  $125 \mu\text{m}$ . Details of the FBG sensing system and sensing principle were described in Zhou *et al* (1999) and Jin *et al* (2000). Since the sensor grating has

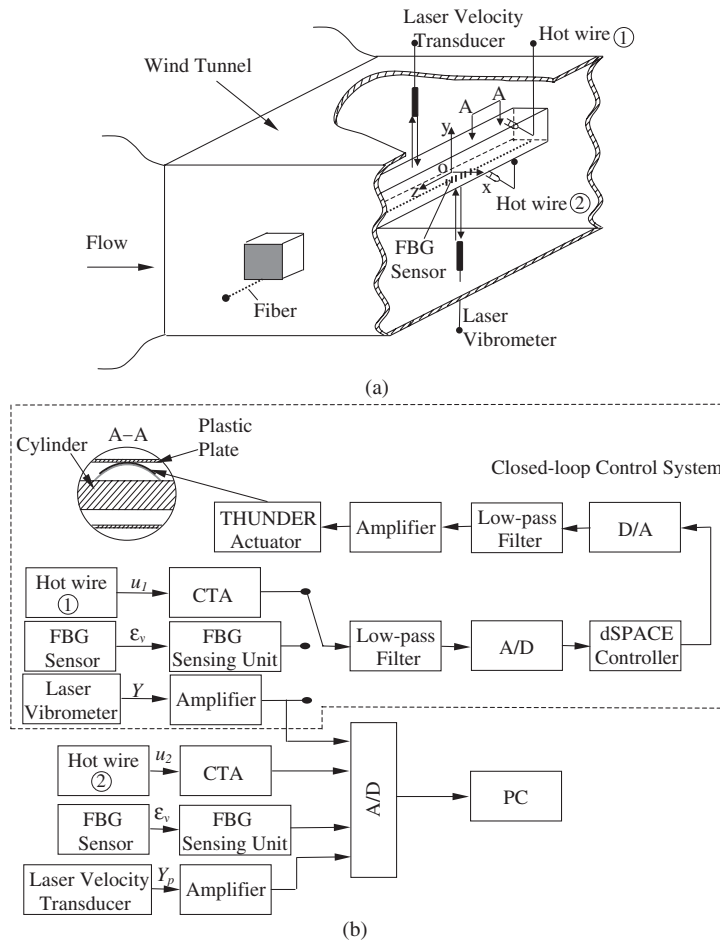


**Figure 3.** Experimental set-up: (a) mechanical and sensing configuration; (b) schematic diagram of the closed-loop control system and measurement system.

a finite length of about 10 mm, the measurement represents an average strain over this spanwise length.

The above measured signals ( $u_1$ ,  $\epsilon_y$  and  $Y$ ) can be used as feedback signals either individually or in combination (figure 3(b)). After amplification, all feedback signals were low pass filtered at a cut-off frequency of 200 Hz and then input into a digital signal processor (DSP) fitted with 16-bit AD and DA converter. The converted analog signals were low pass filtered again (cut-off frequency = 200 Hz) and amplified by two dual-channel piezo-driver amplifiers (Trek PZD 700) before activating the THUNDER actuators. The use of the two low pass filters in the feed-forward and feedback passages was to remove high frequency noises from turbulence and electronic components.

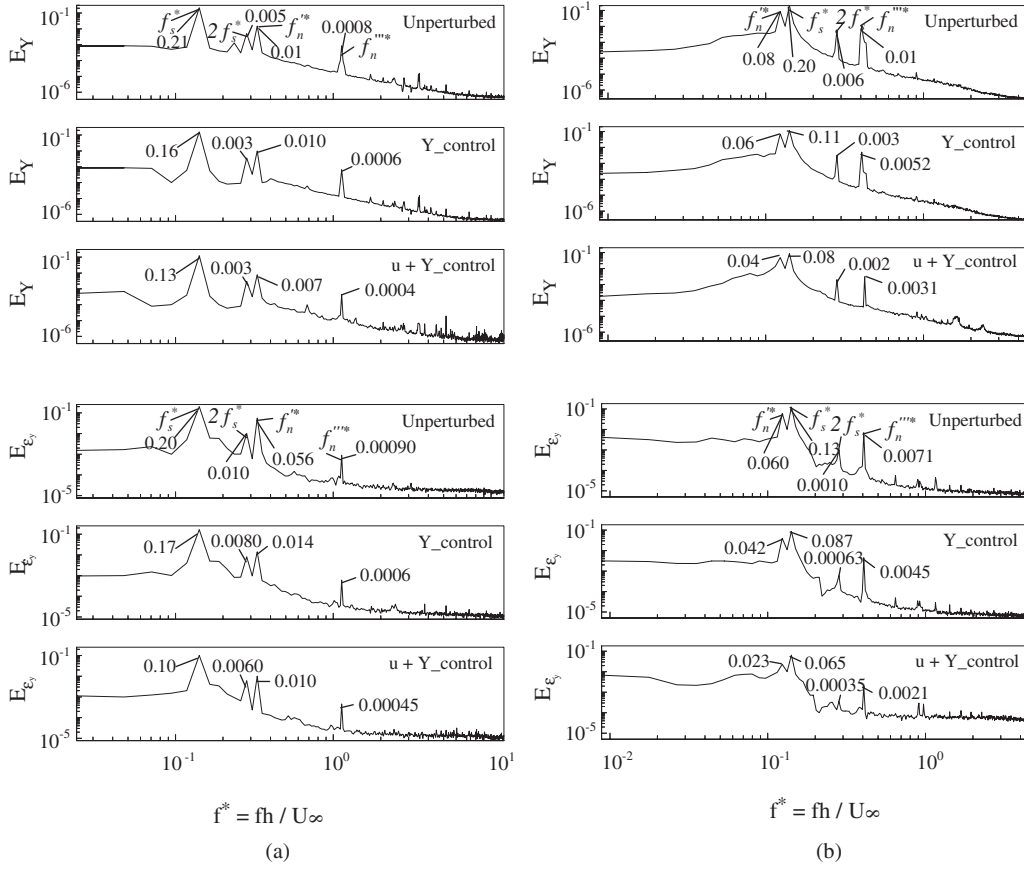
In order to monitor and analyze the control performance, a second 5  $\mu\text{m}$  tungsten hot wire (hot wire ②) was placed at  $x/h = 2$ ,  $y/h = 1.5$ ,  $z = 0$ , where the vortex shedding signal was strong. The measured fluctuating velocity signal ( $u_2$ ), together with  $\epsilon_y$ ,  $Y$  and the surface perturbation displacement  $Y_p$  measured with a B&K laser velocity transducer, was amplified and recorded in a personal computer through a 12-bit AD board at a sampling frequency of 3.5 kHz/channel (figure 3(b)). The duration of each record was 20 s. In addition, the flow structure was measured using a particle

image velocimeter (PIV), which is a Dantec standard PIV2100 system, including a CCD camera for digital particle images and two New Wave standard pulsed laser sources for illumination. The PIV system has a built-in function for flow visualization. Each image covered an area of 176 mm  $\times$  141 mm or  $x/h \approx 0.5$ –10.8 and  $y/h \approx -4.1$ –4.1 of the flow field for both flow visualization and PIV measurements. See Zhang *et al* (2004) for more detailed information on the PIV measurement.

#### 4. Controller design and parameter optimization

Five control schemes, depending on the feedback signals, i.e.  $u_1$ ,  $\epsilon_y$  and  $Y$ , have been investigated. The schemes may be divided into two categories. One is called the one-element control scheme using the single  $u_1$ ,  $\epsilon_y$  or  $Y$ , referred to as  $u$ \_control,  $\epsilon_y$ \_control and  $Y$ \_control, respectively. The other category is called the two-element control scheme, which uses a combination of  $u_1$  and  $\epsilon_y$  or  $u_1$  and  $Y$ , namely,  $u + \epsilon_y$ \_control and  $u + Y$ \_control, respectively.

For each scheme, the design of the feedback controller involves two parameters: a gain coefficient in amplitude ( $\tilde{P}_q$ ) and a phase shift ( $\tilde{\phi}_q$ ) between the output and input of the controller  $q$ , representing  $u_1$ ,  $\epsilon_y$  or  $Y$ . Both  $\tilde{P}_q$  and  $\tilde{\phi}_q$  were manually tuned during experiments to achieve a maximum



**Figure 4.** Effect on the power spectrum of  $Y$  and  $\varepsilon_y$  under the control schemes of  $Y\_control$  and  $u + Y\_control$ , respectively: (a)  $Re = 2800$ ; (b)  $Re = 8000$ .

reduction in the root mean square (rms) value of  $Y$ , i.e.,  $Y_{rms}$ . The procedure is as follows: for the one-element scheme, vary  $\tilde{P}_q$  first by maintaining  $\tilde{\phi}_q = 0^\circ$  to find a  $\tilde{P}_q$ , i.e.,  $\tilde{P}_{q,opt}$ , leading to the smallest  $Y_{rms}$ . Then vary  $\tilde{\phi}_q$  for given  $\tilde{P}_{q,opt}$  within a cycle of  $360^\circ$  to determine the  $\tilde{\phi}_{q,opt}$ , under which  $Y_{rms}$  reaches the minimum.  $\tilde{P}_{q,opt}$  and  $\tilde{\phi}_{q,opt}$  are used as the optimal parameters of the controller. The two-element scheme follows first the same tuning procedure for each feedback signal to obtain an initial configuration. Then, apply simultaneously the two signals determined from the initial configuration as a starting point for fine-tuning, in which both  $\tilde{P}_q$  and  $\tilde{\phi}_q$  are adjusted again for each signal. Several iterations were needed to determine the final configuration, which yields the maximum reduction in  $Y_{rms}$ .

The whole controller design process was carried out using a digital open source platform dSPACE. This platform provides a real-time system for rapid control prototyping, production code generation and hardware-in-the-loop tests. A digital signal processor (DSP) with the SIMULINK function of MATLAB and software (ControlDesk 2.0) was used for sampling and processing feedback signals.

The tuning process led to an optimal configuration for each scheme with optimal parameters under two  $Re$  cases. As an example, two optimal control schemes, i.e.  $Y\_control$  and  $u + Y\_control$ , are discussed in this paper with optimal parameters tabulated in table 1.

**Table 1.** Optimal  $\tilde{P}_q$  and  $\tilde{\phi}_q$  ( $q$  represents  $u_1$  or  $Y$ ) under different control schemes.

Optimal parameter	Control scheme			
	$Re = 2800$		$Re = 8000$	
	$Y\_control$	$u + Y\_control$	$Y\_control$	$u + Y\_control$
$\tilde{P}_{u_1}$		3.5		4
$\tilde{\phi}_{u_1}$		$100^\circ$		$120^\circ$
$\tilde{P}_Y$	3	8	8	5
$\tilde{\phi}_Y$	$120^\circ$	$95^\circ$	$144^\circ$	$80^\circ$

## 5. Control performances

### 5.1. Effect on structural vibration

Figure 4 shows the power spectral density functions,  $E_Y$  and  $E_{\varepsilon_y}$ , of  $Y$  and  $\varepsilon_y$  with and without control. The spectrum of fluctuation  $\alpha$ , representing  $Y$  or  $\varepsilon_y$ , has been normalized such that  $\int_0^\infty E_\alpha(f) df = 1$ . In the absence of perturbation,  $E_Y$  or  $E_{\varepsilon_y}$  displays four pronounced peaks at  $f_s^*$ ,  $2f_s^*$ ,  $f_n^*$  and  $f_n^{***}$  for either  $Re$  (figures 4(a) and (b)). Unless otherwise stated, the asterisk denotes normalization by  $h$  and  $U_\infty$ , for example,  $f^* = fh/U_\infty$ . Due to anti-symmetry about the mid-span of the cylinder, the second-mode vibration of the cylinder is not expected. When the  $Y\_control$  scheme is deployed, there is a

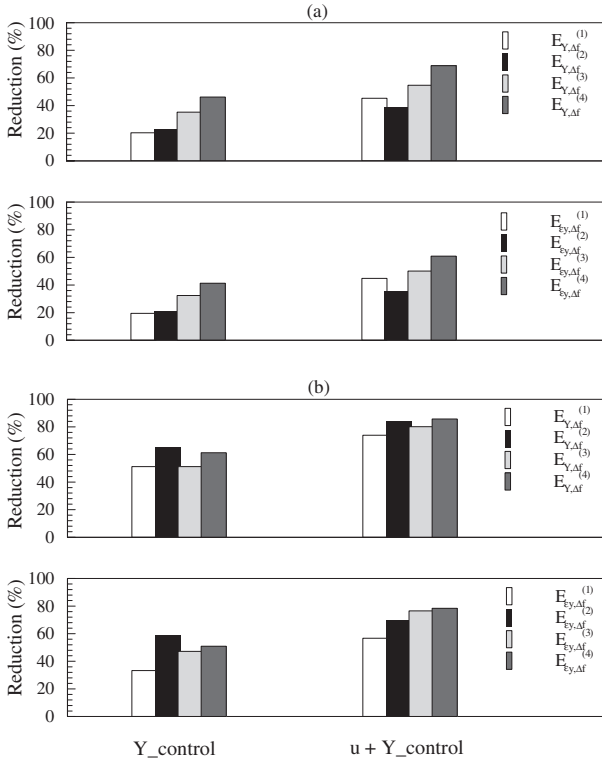


**Figure 5.** Reduction in  $E_{Y,\Delta f}^{(n)}$  and  $E_{\varepsilon_y,\Delta f}^{(n)}$  ( $n = 1, 2, 3, 4$ ). (a)  $Re = 2800$ ; (b)  $Re = 8000$ .

significant reduction in amplitude of the peaks in both  $E_Y$  and  $E_{\varepsilon_y}$ . Using the  $u + Y\_control$  scheme, the reduction is further improved. For instance, at  $Re = 8000$  (figure 4(b)), the peak amplitudes drop by 60%, 67%, 50% and 62% at  $f_s^*$ ,  $2f_s^*$ ,  $f_n^*$  and  $f_n^{***}$ , respectively, in  $E_Y$  and the corresponding drops are 50%, 65%, 62% and 70%, respectively, in  $E_{\varepsilon_y}$ . The results indicate the effectiveness of the control.

The control effect may be further estimated, on the energies in  $E_Y$  and  $E_{\varepsilon_y}$  associated with frequencies at  $f_s^*$ ,  $2f_s^*$ ,  $f_n^*$  and  $f_n^{***}$ , i.e.,  $E_{Y,\Delta f}^{(n)}$  and  $E_{\varepsilon_y,\Delta f}^{(n)}$  ( $n = 1, 2, 3, 4$ ), which are calculated by integrating the power spectral density functions over  $-3$  dB bandwidth centered about the peaks and subsequently multiplying with  $Y_{rms}$  or  $\varepsilon_{y,rms}$ . The results are given in figure 5. It is evident that the energies of structural vibration associated with the four frequencies all undergo significant decrease, indicating the suppression of the cylinder oscillation. The  $u + Y\_control$  scheme apparently outperforms the  $Y\_control$  scheme. This is evident in the time histories of  $Y$  and  $\varepsilon_y$  (figure 6). Furthermore, at  $Re = 8000$  (figures 5(b) and 6(b)), the former achieves a reduction between 75% and 86% in  $E_{Y,\Delta f}^{(1)}$ ,  $E_{Y,\Delta f}^{(2)}$ ,  $E_{Y,\Delta f}^{(3)}$  and  $E_{Y,\Delta f}^{(4)}$ , and between 57% and 79% in  $E_{\varepsilon_y,\Delta f}^{(1)}$ ,  $E_{\varepsilon_y,\Delta f}^{(2)}$ ,  $E_{\varepsilon_y,\Delta f}^{(3)}$  and  $E_{\varepsilon_y,\Delta f}^{(4)}$ . The corresponding reduction is 58% and 52% in the amplitude of  $Y$  and  $\varepsilon_y$ , respectively. On the other hand, the latter scheme only yields a reduction between 52% and 65% in  $E_{Y,\Delta f}^{(1)}$ ,  $E_{Y,\Delta f}^{(2)}$ ,  $E_{Y,\Delta f}^{(3)}$  and  $E_{Y,\Delta f}^{(4)}$ , and between 33% and 60% in  $E_{\varepsilon_y,\Delta f}^{(1)}$ ,  $E_{\varepsilon_y,\Delta f}^{(2)}$ ,  $E_{\varepsilon_y,\Delta f}^{(3)}$  and  $E_{\varepsilon_y,\Delta f}^{(4)}$ . The reduction is 37% and 31% in the amplitude of  $Y$  and  $\varepsilon_y$ , respectively.

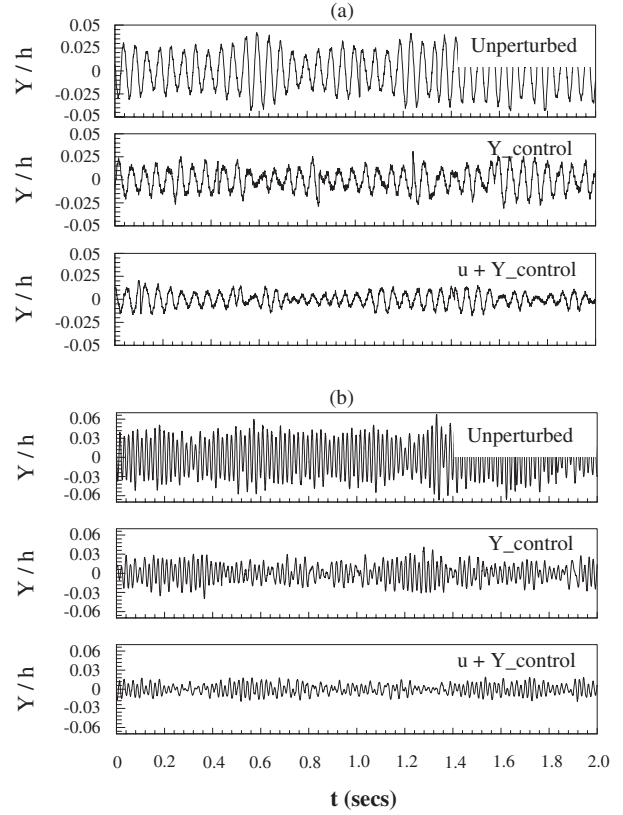
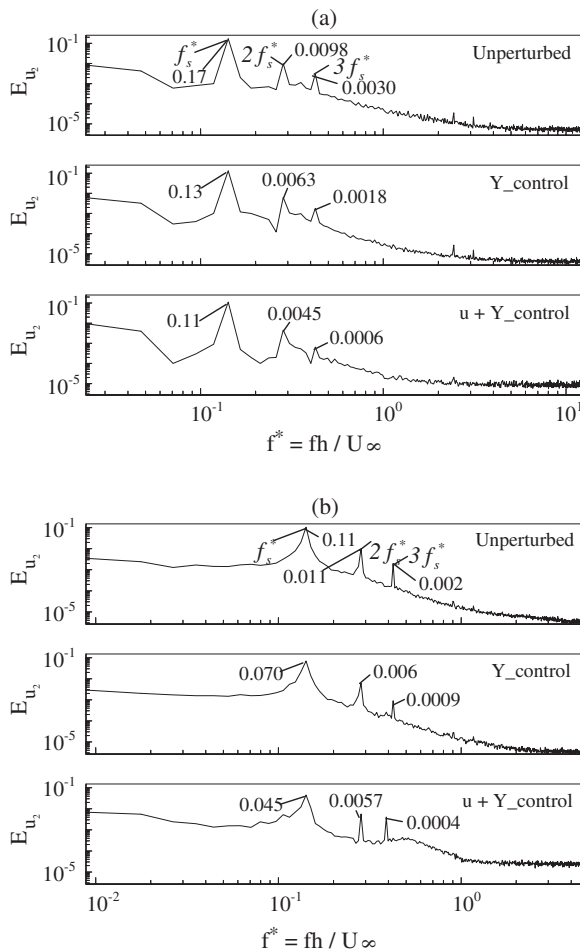


**Figure 6.** Typical time histories of  $Y$  under the control schemes of  $Y\_control$  and  $u + Y\_control$ , respectively: (a)  $Re = 2800$ ; (b)  $Re = 8000$ . The time origin was arbitrary.

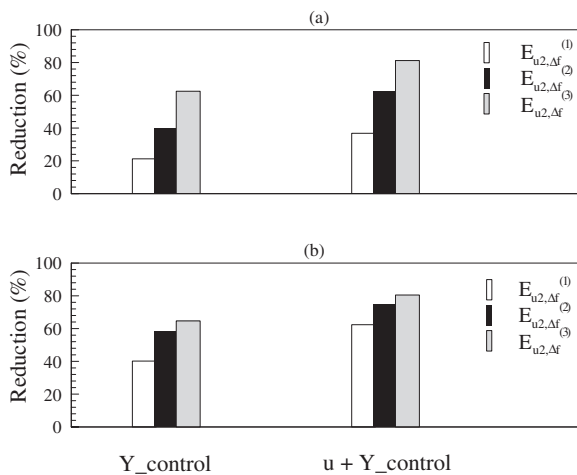
### 5.2. Effect on vortex shedding

Figure 7 shows the  $u_2$ -spectrum,  $E_{u_2}$ . In the absence of perturbation,  $E_{u_2}$  displays peaks at  $f_s^*$ ,  $2f_s^*$  and  $3f_s^*$ . Once perturbed, these peaks are all suppressed to different extents. Figure 8 presents quantitatively the reduction, compared with the absence of perturbation, in the energies of  $E_{u_2}$  associated with  $f_s^*$ ,  $2f_s^*$  and  $3f_s^*$ , i.e.,  $E_{u_2,\Delta f}^{(n)}$  ( $n = 1, 2, 3$ ) and figure 9 shows the typical time histories of  $u_2$ . Again, the  $u + Y\_control$  scheme outperforms the  $Y\_control$  scheme. The former achieves a reduction by 37%, 62%, 81% and 42% in  $E_{u_2,\Delta f}^{(1)}$ ,  $E_{u_2,\Delta f}^{(2)}$ ,  $E_{u_2,\Delta f}^{(3)}$  and  $u_{2,rms}$ , respectively, at  $Re = 2800$  and by 62%, 74%, 81% and 53%, respectively, at  $Re = 8000$ . The latter yields a reduction by 22%, 40%, 62% and 19% in  $E_{u_2,\Delta f}^{(1)}$ ,  $E_{u_2,\Delta f}^{(2)}$ ,  $E_{u_2,\Delta f}^{(3)}$  and  $u_{2,rms}$ , respectively, at  $Re = 2800$  and by 41%, 58%, 65% and 36%, respectively, at  $Re = 8000$ .

Figures 10 and 11 show typical flow visualization photos (left column) and iso-contours of spanwise vorticity (right column) measured using PIV. The solid square in the figures indicates the cylinder position. Without control, the Kármán vortex street is evident in figures 10(a) and 11(a). Once control is introduced, vortex shedding from the cylinder and the normalized maximum spanwise vorticity,  $|\omega_{z,max}^*| = |\omega_{z,max}|h/U_\infty$ , are weakened, as is evident in figures 10(b), (c) and 11(b), (c); vortices appear to be breaking up, showing considerably less coherence and weaker strength. The  $u + Y\_control$  scheme shows better performance than the  $Y\_control$  scheme,  $|\omega_{z,max}^*|$  decreasing by 36% ( $Re = 2800$ ) and 54%



**Figure 7.** Effect on the power spectrum of  $u_2$  under the control schemes of  $Y\_control$  and  $u + Y\_control$ , respectively: (a)  $Re = 2800$ ; (b)  $Re = 8000$ .



**Figure 8.** Reduction in  $E_{u_2, \Delta f}^{(n)}$  ( $n = 1, 2, 3$ ). (a)  $Re = 2800$ ; (b)  $Re = 8000$ .

( $Re = 8000$ ), respectively, for the former and by 18% ( $Re = 2800$ ) and 31% ( $Re = 8000$ ) for the latter.

The overall performances of the closed-loop control are summarized in table 2. Evidently, irrespective of  $Re$  and

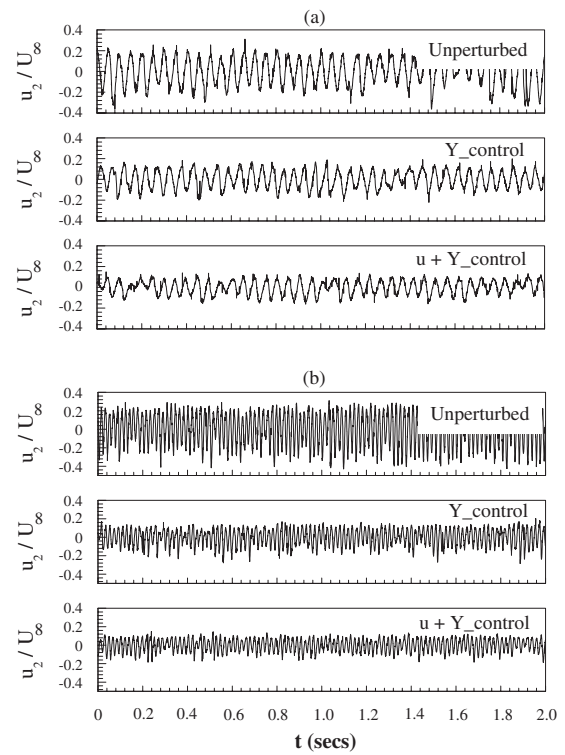


**Figure 9.** Typical time histories of  $u_2$  under the control schemes of  $Y\_control$  and  $u + Y\_control$ , respectively: (a)  $Re = 2800$ ; (b)  $Re = 8000$ . The time origin was arbitrary.

**Table 2.** Control performance under two  $Re$  cases.

Control effect	Control scheme			
	$Re = 2800$		$Re = 8000$	
	$Y\_control$	$u + Y\_control$	$Y\_control$	$u + Y\_control$
$Y_{rms}$	24%↓	43%↓	37%↓	58%↓
$\varepsilon_{y,rms}$	20%↓	39%↓	31%↓	52%↓
$u_{2,rms}$	19%↓	42%↓	36%↓	53%↓
$\Gamma$	45%↓	79%↓	54%↓	88%↓
$V_{p,rms}$	92 V	60 V	75 V	55 V

the control schemes, the root mean square values of  $Y$ ,  $\varepsilon_y$  and  $u_2$ , i.e.  $Y_{rms}$ ,  $\varepsilon_{y,rms}$  and  $u_{2,rms}$ , and circulation  $\Gamma$  are all reduced to different extents. The circulation  $\Gamma$  was estimated as  $\frac{\Gamma}{U_\infty h} = \sum_{i,j} (\omega_z^*)_{ij} \frac{\Delta A}{h^2}$  (Brian and Donald 1983) with a cut-off level of 0.3, about 10% of  $|\omega_{z,max}^*|$ , as used by Sumner *et al* (2000).  $u + Y\_control$  outperforms  $Y\_control$  in every category, resulting in a higher reduction in  $Y_{rms}$ ,  $\varepsilon_{y,rms}$ ,  $u_{2,rms}$  and  $\Gamma$  despite the smaller root mean square value of the perturbation voltage  $V_p$ . For example, at  $Re = 8000$ , the required  $V_{p,rms}$  for  $u + Y\_control$  is 55 V as opposed to 75 V needed for  $Y\_control$ . Since the resistance of the actuation channel remains the same in the two cases, a smaller  $V_{p,rms}$  means a lower energy input. This indicates one great advantage of the closed-loop control, i.e., the possibility of developing a more compact, self-contained and low energy control system, in particular if the  $u + Y\_control$  scheme is applied.

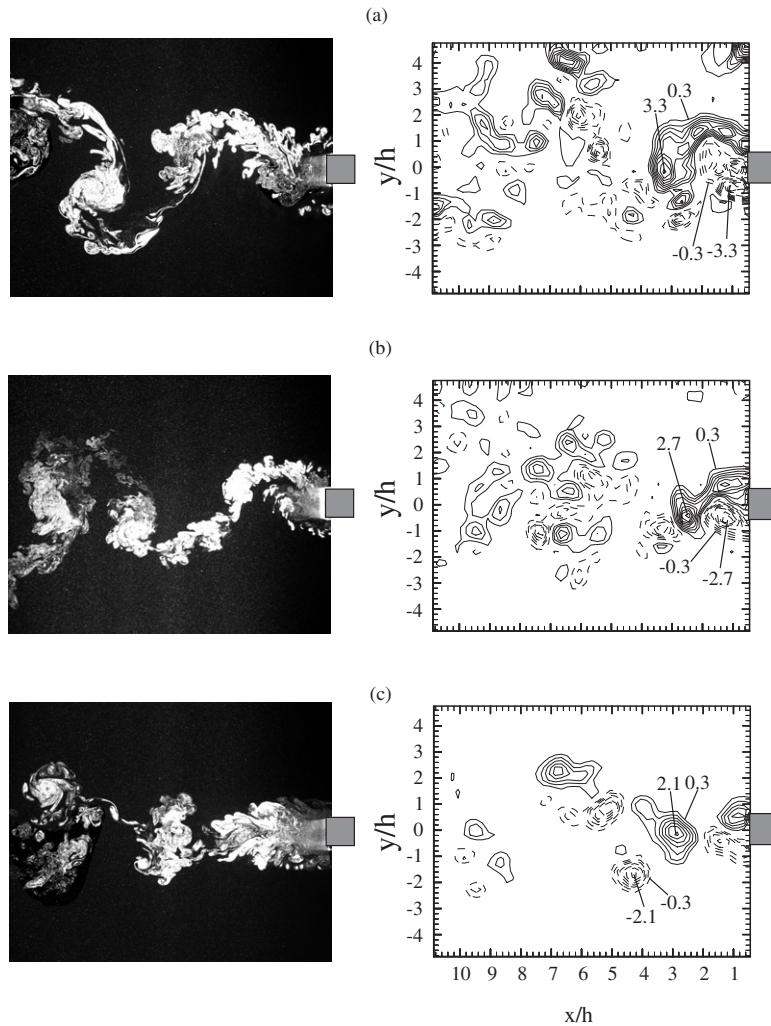


**Figure 10.** Typical flow visualization photographs and PIV measured iso-contours of spanwise vorticity  $\omega_z^* = \omega_z h / U_\infty$  with and without control: (a) unperturbed; (b)  $Y\_control$ ; (c)  $u + Y\_control$ .  $Re = 2800$ .

### 6. Discussion

To understand the physics behind weakened vortex shedding and associated structural vibration, the spectral phase, i.e.  $\phi_{Y u_2} \equiv \tan^{-1}(Q_{Y u_2} / Co_{Y u_2})$ , between the simultaneously measured  $Y$  and  $u_2$  is calculated and this is shown in figures 12 and 13 for the two  $Re$  values, where  $Co_{Y u_2}$  and  $Q_{Y u_2}$  stand for the cospectrum and quadrature spectrum of  $Y$  and  $u_2$ , respectively.

As discussed in Cheng *et al* (2003),  $\phi_{Y u_2}$  indicates approximately the phase relationship between the lateral structural oscillating velocity,  $\dot{Y}$ , and the lateral velocity,  $v$ , of the flow around the cylinder. Thus,  $\phi_{Y u_2} = 0$  and  $-\pi$  indicate synchronized and opposite movements between  $\dot{Y}$  and  $v$ , respectively. Without perturbation,  $\phi_{Y u_2}$  is about zero near  $f_s^*$ ,  $2f_s^*$ ,  $f_n^*$  and  $f_n^{***}$  (figures 12(a) and 13(a)), that is,  $\dot{Y}$  and  $v$  are almost synchronized at these frequencies. The plateaus around  $f_s^*$ ,  $2f_s^*$ ,  $f_n^*$  and  $f_n^{***}$  show that the synchronization occurs over a range of frequencies. However,  $\phi_{Y u_2}$  at these frequencies is changed from 0 to near  $-\pi$  under  $Y\_control$  and  $u + Y\_control$  schemes (figures 12(b), (c) and 13(b), (c)), implying that  $\dot{Y}$  and  $v$  collide or move against each other. In other words, the

synchronized fluid–structure interaction at the four frequencies is effectively destroyed, resulting in simultaneous impairment in vortex shedding and structural vibration. This phase change is more extensive under the  $u + Y\_control$  scheme for  $f_s^*$ ,  $2f_s^*$ ,  $f_n^*$  and  $f_n^{***}$  than the  $Y\_control$  scheme, conforming with the superior control performance of the former over the latter.

The present investigation focuses on controlling the flow-induced vibration on a fix-supported flexible cylinder. We have previously conducted similar work on a rigid structure flexibly supported at both ends (Zhang *et al* 2004) or a rigid structure fix-supported at both ends (Zhang *et al* 2005). Of course, flow control is the primary purpose for the latter publication. There is a difference in control between the rigid and flexible structure cases. The former involves the control of only the first-mode vibration, while the latter involves the control of the vibration of multiple modes. Since it is difficult, or impossible, to maintain the experimental conditions (e.g. experimental set-up, Reynolds number), the parameters of the controller and the perturbation amplitude etc the same for the two cases, it is unreasonable to compare the results of the two cases quantitatively. Nevertheless, the two cases share a similarity in the physics of control: the structural vibration and

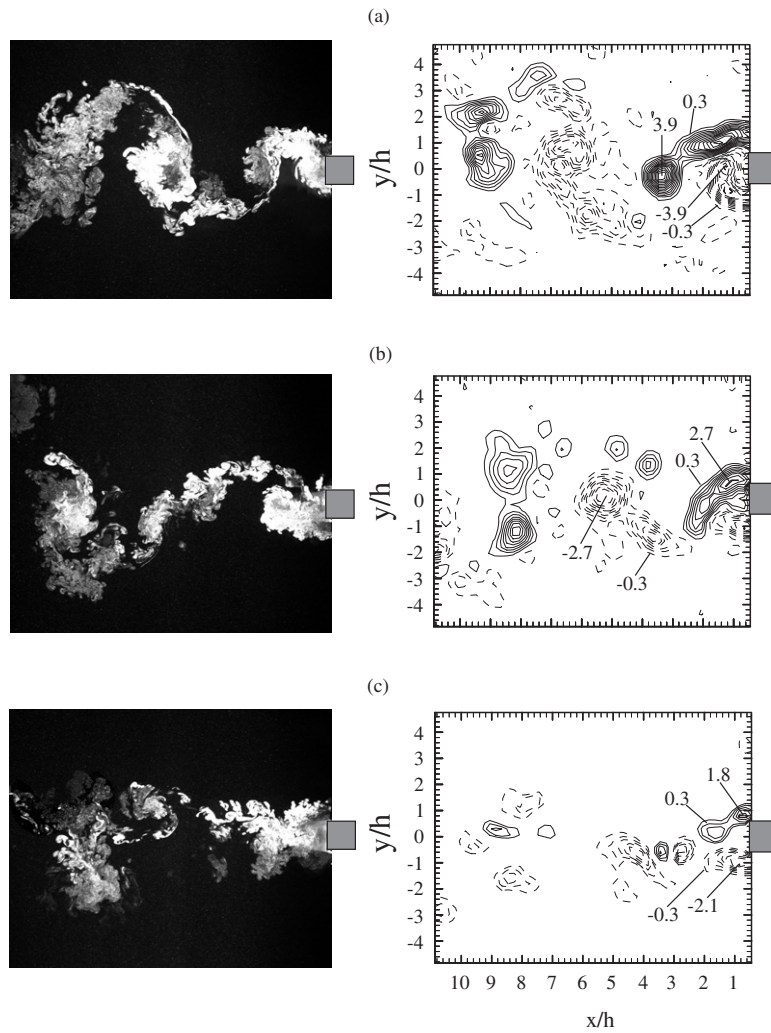


**Figure 11.** Typical flow visualization photographs and PIV measured iso-contours of the spanwise vorticity  $\omega_z^* = \omega_z h / U_\infty$  with and without control: (a) unperturbed; (b)  $Y\_control$ ; (c)  $u + Y\_control$ .  $Re = 8000$ .

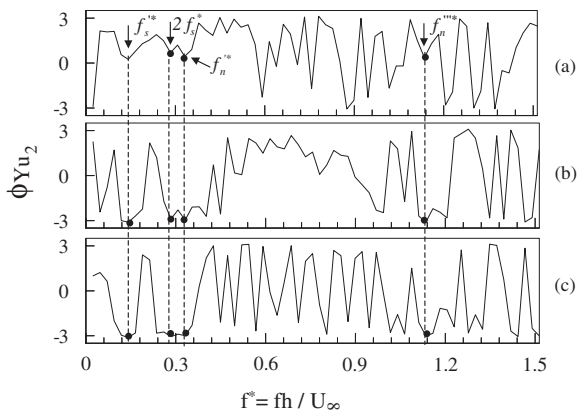


**Figure 12.** Phase shift  $\phi_{Yu_2}$  between structural vibration ( $Y$ ) and fluctuating streamwise flow velocity ( $u_2$ ) under different control schemes: (a) unperturbed; (b)  $Y\_control$ ; (c)  $u + Y\_control$ .  $Re = 2800$ .

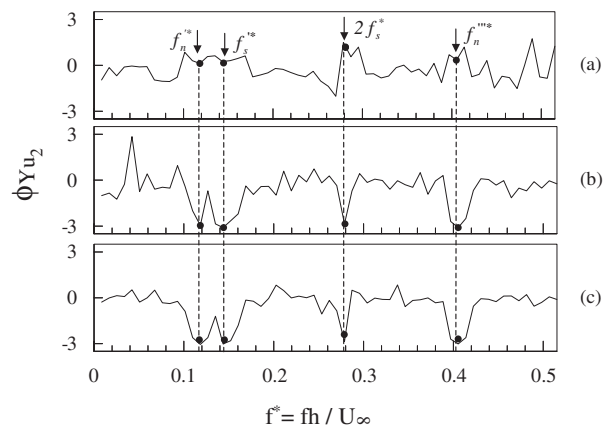


**Figure 13.** Phase shift  $\phi_{Yu_2}$  between structural vibration ( $Y$ ) and fluctuating streamwise flow velocity ( $u_2$ ) under different control schemes: (a) unperturbed; (b)  $Y\_control$ ; (c)  $u + Y\_control$ .  $Re = 8000$ .

vortex shedding are synchronized or in phase at the dominant frequencies without control, but become in anti-phase in the

presence of control, that is, the nature of the fluid–structure interaction has been changed from reinforcing at the dominant

frequencies to dissipating, resulting in greatly weakened vortex shedding and subsequently induced structural vibration.

## 7. Conclusions

The closed-loop control was successfully implemented to suppress the vortex-induced non-resonance vibration on a flexural cylinder using piezo-ceramic actuators. Two typical control schemes, namely,  $Y_{\text{control}}$  and  $u + Y_{\text{control}}$ , were investigated, which used structural vibration ( $Y$ ) and a combination of  $Y$  and flow velocity ( $u$ ) for feedback signals, respectively. It has been shown that the non-resonant multi-mode vibration can be effectively controlled using the present technique; the  $u + Y_{\text{control}}$  scheme is seen to reduce  $Y_{\text{rms}}$ ,  $\varepsilon_{y,\text{rms}}$ ,  $u_{2,\text{rms}}$  and  $\Gamma$  at  $Re = 8000$  by 58%, 52%, 53% and 88%, respectively, compared with their counterparts in the absence of control. The control changes the phase shift between the structural vibration and flow from in phase to in anti-phase. Correspondingly, the synchronized motion between the fluid and structure at  $f_s^*$ ,  $2f_s^*$ ,  $f_n^*$  and  $f_n^{***}$  changes to collision, accounting for the simultaneously attenuated structural vibration and vortex shedding.

## Acknowledgment

The authors wish to acknowledge support given to them by a grant from the Research Grants Council of Hong Kong Special Administrative Region, China (Project Nos PolyU 1/02C and PolyU 5294/03E).

## References

- Baz A and Kim M 1993 Active modal control of vortex-induced vibrations of a flexible cylinder *J. Sound Vib.* **165** 69–84
- Bearman P W 1967 On vortex street wakes *Fluid Mech.* **28** 625–41
- Blevins R D 1985 The effect of sound on vortex shedding from cylinders *J. Fluid Mech.* **161** 217–37
- Brian C and Donald C 1983 An experimental study of entrainment and transport in the turbulent near wake of a circular cylinder *J. Fluid Mech.* **136** 321–74
- Cheng L, Zhou Y and Zhang M M 2003 Perturbed interaction between vortex shedding and induced vibration *J. Fluids Struct.* **17** 887–901
- Copeland B M, Buckley J D, Bryant R G, Fox R L and Hellbaum R F 1999 *THUNDER—an Ultra-High Displacement Piezoelectric Actuator* NASA Langley Research Center, Hampton, VA
- Ffowcs Williams J E and Zhao B C 1989 The active control of vortex shedding *J. Fluids Struct.* **3** 115–22
- Filler J R, Marston P L and Mih W C 1991 Response of the shear layers separating from the circular cylinder to small amplitude rotational oscillations *J. Fluid Mech.* **231** 481–99
- Gao J X and Cheng L 2004 Modelling of a high performance piezoelectric actuator assembly for active and passive vibration control *Smart Mater. Struct.* **13** 384–92
- Griffin O M and Ramberg S E 1975 On vortex strength and drag in bluff-body wakes *J. Fluid Mech.* **69** 721–28
- Halim D and Moheimani S O R 2002 Spatial H-2 control of a piezoelectric laminate beam: experimental implementation *IEEE Trans. Control Syst. Technol.* **10** 533–46
- Hsiao F B and Shyu J Y 1991 Influence of internal acoustic excitation upon flow passing a circular cylinder *J. Fluids Struct.* **5** 427–42
- Huang X Y 1996 Feedback control of vortex shedding from a circular cylinder *Exp. Fluids* **20** 218–24
- Jin W, Zhou Y, Chan P K C and Xu H G 2000 A fibre-optic grating sensor for the study of flow-induced vibrations *Sensors Actuators* **79** 36–45
- Jung W J, Mangiavacchi N and Akhavan R 1992 Suppression of turbulence in wall-bounded flows by high-frequency spanwise oscillations *Phys. Fluids A* **4** 1605–7
- Koopman G H 1967 The vortex wakes of vibrating cylinders at low Reynolds numbers *J. Fluid Mech.* **28** 501–12
- Min C H and Choi H C 1999 Suboptimal feedback control of vortex shedding at low Reynolds numbers *J. Fluid Mech.* **401** 123–56
- Mittal S and Kumar V 2001 Flow-induced vibrations of a light circular cylinder at Reynolds numbers 10(3) to 10(4) *J. Sound Vib.* **245** 923–46
- Owen J C, Bearman P W and Szweczyk A A 2001 Passive control of viv with drag reduction *J. Fluids Struct.* **15** 597–605
- Provansal M, Mathis C and Boyer L 1987 Benard–von Kármán instability: transient and forced regimes *J. Fluid Mech.* **182** 1–22
- Roussopoulos K 1993 Feedback control of vortex shedding at low Reynolds numbers *J. Fluid Mech.* **248** 267–96
- Sarpkaya T 2004 A critical review of intrinsic nature of vortex-induced vibrations *J. Fluids Struct.* **19** 389–447
- Sumner D, Price S J and Paidoussis M P 2000 Flow-pattern identification for two staggered circular cylinders in cross-flow *J. Fluid Mech.* **411** 263–303
- Tani J, Qiu J and Liu Y 1999 Robust control of vortex-induced vibration of a rigid cylinder supported by an elastic beam using  $\mu$ -synthesis *J. Fluids Struct.* **13** 865–75
- Tokumaru P T and Dimotakis P E 1991 Rotary oscillation control of a cylinder wake *J. Fluid Mech.* **224** 77–90
- Unal M F and Rockwell D 1988a On vortex formation for a cylinder. Part 1. The initial instability *J. Fluid Mech.* **190** 491–512
- Unal M F and Rockwell D 1988b On vortex formation from a cylinder. Part 2. Control by splitter plate interference *J. Fluid Mech.* **190** 513–29
- Williams D R, Mansy H and Amato C 1992 The response and symmetry properties of a cylinder wake subjected to localized surface excitation *J. Fluid Mech.* **234** 71–96
- Williamson C H K and Roshko A 1988 Vortex formation in the wake of an oscillating cylinder *J. Fluids Struct.* **2** 355–81
- Winkel E S, Ceccio S L, Dowling D R and Perlin M 2004 Bubble-size distributions produced by wall injection of air into flowing freshwater, saltwater and surfactant solutions *Exp. Fluids* **37** 802–10
- Yang S M and Chen C W 1996 Application of single mode optical fiber sensors in structural vibration suppression *J. Intell. Mater. Syst. Struct.* **7** 71–7
- Zdravkovich M M 1981 Review and classification of various aerodynamic and hydrodynamic means for suppressing vortex shedding *J. Wind Eng. Ind. Aerodyn.* **7** 145–89
- Zhang H J, Zhou Y, So R M C, Mignolet M P and Wang Z J 2003 A note on the fluid damping of an elastic cylinder in a cross flow *J. Fluids Struct.* **17** 479–83
- Zhang M M, Cheng L and Zhou Y 2004 Closed-loop-controlled vortex shedding from a flexibly supported square cylinder under different schemes *Phys. Fluids* **16** 1439–48
- Zhang M M, Cheng L and Zhou Y 2005 Closed-loop manipulation of vortex shedding from a fixed-supported square cylinder *Exp. Fluids* **39** 75–85
- Zhou Y, So R M C, Jin W, Xu H G and Chan P K C 1999 Dynamic strain measurements of a circular cylinder in a cross flow using a fibre Bragg grating sensor *Exp. Fluids* **27** 359–67
- Zhou Y, Wang Z J, So R M C, Xu S J and Jin W 2001 Free vibrations of two side-by-side cylinders in a cross flow *J. Fluid Mech.* **443** 197–229